PERGAMON

Journal of Structural Geology 25 (2003) 317–331

JOURNAL OF STRUCTURAL GEOLOGY

www.elsevier.com/locate/jsg

Cataclasis and particulate flow in faulted, poorly lithified sediments

Geoffrey C. Rawling*, Laurel B. Goodwin

Department of Earth and Environmental Science, New Mexico Tech, Socorro, NM 87801, USA

Received 21 February 2002; accepted 5 March 2002

Abstract

Microscopic observations of normal faults in poorly lithified sediments from the Rio Grande rift, New Mexico, USA, reveal that the mode of grain fracture within the fault zones is controlled by mineralogy and relative grain strength. Transgranular fracturing of quartz is rarely observed—quartz typically deforms by flaking of grain edges, feldspar by transgranular fracture facilitated by easy cleavage, and lithic fragments by transgranular fracture or distributed microcracking. Particle size measurements indicate that progressive deformation produces a particle size distribution that can be described by a power-law model, characterized by low D values (1.7–2.1). This indicates a preponderance of large particles with respect to cataclasite produced by constrained comminution ($D \sim 2.6$). We interpret these results in terms of cataclastic deformation by controlled particulate flow under low confining pressure, in which extensive transgranular fracturing is not necessary for strain accumulation. This style of cataclastic deformation is different from that observed in crystalline and well lithified sedimentary rocks. It is in part responsible for the characteristic internal structure and hydrologic properties of normal faults in poorly lithified sediments, and thus has implications for diagenetic processes and interpreting fault zone deformation history.

Keywords: Cataclasis; Faults; Sediments; Particulate flow

1. Introduction

Brittle faulting of porous sediments and sedimentary rocks in the shallow crust is accomplished by cataclasis, a deformation mechanism which "…involves the brittle fragmentation of mineral grains with rotation of grain fragments accompanied by frictional grain boundary sliding and dilatancy" (Sibson, 1977). There is abundant evidence from field studies of faults in sandstones that cataclasis is the dominant low temperature deformation mechanism in sedimentary rocks, both in small displacement faults or deformation bands (Aydin, 1978; Underhill and Woodcock, 1987; Antonellini et al., 1994) and large displacement fault zones (Engelder, 1974; Blenkinsop and Rutter, 1986). This has been verified through experimental deformation of sandstones (e.g. Dunn et al., 1973; Menéndez et al., 1996; Wong et al., 1997).

Compared with lithified sandstones, there have been few studies of cataclasis in unlithified sediments. Antonellini et al. (1994) suggested that deformation bands in lithified sandstones formed without cataclasis under low normal stress conditions when the sandstones were not fully lithified. However, Lucas and Moore (1986) documented extensive cataclasis that occurred in accretionary wedges when the sediments were partially lithified. Hooke and Iverson (1995) presented evidence for cataclasis in deformed glacial till. Although primarily concerned with fault-zone cementation and effects of faults on fluid flow, Mozley and Goodwin (1995), Heynekamp et al. (1999), and Sigda et al. (1999) noted evidence for cataclasis in studies of faults in poorly lithified sediments. Recently, Cashman and Cashman (2000) documented cataclasis in deformation bands in unlithified Pleistocene sands, and argued that they formed under very low confining pressure, possibly during seismic slip events. Cataclasis has been observed in laboratory deformation of various granular materials and sand (Borg et al., 1960; Mandl et al., 1977; Marone and Scholz, 1989; Been et al., 1991).

The particle size distribution (PSD) of cataclastically deformed materials is of particular importance for elucidating the micromechanics of the deformation process. Sammis et al. (1987) investigated the PSD over four orders of magnitude of grain size in gouge from a large-displacement fault in crystalline rock. They concluded that the gouge was self-similar, or fractal, in terms of the number of particles versus their size. Mathematically, this means that the relationship

* Corresponding author. Now at: New Mexico Bureau of Geology and Mineral Resources, 801 Leroy Place, Socorro, NM 87801-4796, USA. Tel.: +1-505-835-5420; fax: +1-505-835-6333.

E-mail addresses: grawling@nmt.edu (G.C. Rawling), lgoodwin@nmt.edu (L.B. Goodwin).

0191-8141/03/$ - see front matter
PII: S0191-8141(02)00041-X

between particle frequency and size can be described by a power law relationship in which the number of particles larger than a given size versus that size plots as a straight line on a double log plot. The slope of the plot is the power law exponent, D, often referred to as the fractal dimension. Sammis et al. (1987) proposed a simple constrained comminution model for gouge development in which the probability of particle fracture is independent of its size or strength but strongly dependent on the size of its nearest neighbors. In the model, when two particles of equal size come into contact, one will fracture. Particles with nearest neighbors of similar sizes are most likely to fracture. Particles break into eight equal-sized subparticles, seven of which break again etc., ultimately yielding a statistically self-similar gouge with a three-dimensional fractal dimension of $D \sim 2.6$. This results in a characteristic microstructure of relict grains surrounded by a matrix of comminution debris, in which no two particles of similar size are nearest neighbors.

Blenkinsop (1991) measured the PSD of gouges from crystalline and lithified sedimentary rocks and observed D values from 1.88 to 3.08. In a study of gouges derived from crystalline rocks from three faults in Southern California, An and Sammis (1994) observed that PSDs for the smaller particles are generally consistent with a power law, or fractal, distribution with D values of 2.5–3.0. The fractal distributions broke down at larger particle sizes. Marone and Scholz (1989) deformed an artificial gouge of Ottawa sand between steel blocks to varying strains. The D value of the resulting PSDs increased with increasing shear strain and reached a plateau of ~2.6 at a shear strain of about 2, supporting the constrained comminution model of Sammis et al. (1987). However, they observed larger D values and smaller average grain sizes in localized, Reidel shear zones. They also observed a breakdown of the fractal PSD within the shear bands that was consistent with the smaller particles having greater fracture strength than the larger particles. This invalidates the size-independent strength of particles required by the Sammis et al. (1987) model, and suggests that the grinding limit had been reached within the Riedel shear zones.

In most studies, the actual process of cataclasis under lithostatic compaction or shear deformation has been observed to be transgranular fracturing initiated by loading at grain-to-grain contacts (e.g. Zhang et al., 1990; Antonellini et al., 1994; Menéndez et al., 1996). Exceptions include Hooke and Iverson (1995), who suggested that abrasion, flaking, or spalling from grain edges was the mode of fracturing in deformed glacial till; Marone and Scholz (1989), who observed that hydrostatically compressed gouge particles showed fracture dominantly along their edges; and Blenkinsop (1991), who related low D values (<2) to in-situ alteration, intermediate D values ($2 < D < 3$) to deformation by constrained comminution and high D values (>3) to selective fracture of large particles after strain localization.

The above discussion focuses on the nature and occurrence of grain fracturing. The other component of cataclasis as defined by Sibson (1977) is frictional grain boundary sliding. Borradaile (1981) treated cataclasis as a particular example of the more general deformation mechanism of particulate flow, of which he identified three types. Independent particulate flow involves grain boundary sliding with no intragranular deformation. Dependent particulate flow occurs when grains cannot move relative to one another unless there is intragranular deformation, such as crystal plasticity, diffusive mass transfer, or fracturing. In controlled particulate flow, the rate of grain boundary sliding is controlled by intragranular deformation, but the amount of sliding of any individual grain is not limited by this deformation. Other workers, (e.g. Porter et al., 2000) use the term particulate flow more generally to refer to deformation accommodated by frictional sliding alone, with no grain breakage or other deformation.

The critical/steady state line determined in soil mechanics tests is the locus of points in porosity–stress invariant space towards which soils and unlithified sediments evolve during progressive deformation. It is useful for characterizing the geotechnical properties and deformation behavior of such materials, for example, the degree of mobilization of debris flows (Ellen and Fleming, 1987). The onset of cataclasis in sands induces a strong curvature to the critical/steady state line (Been et al., 1991). In addition, Sigda et al. (1999) showed that isolated cataclastic deformation bands have two to three orders of magnitude lower permeability than their poorly lithified host sands. Thus, it is apparent that cataclasis affects both the mechanical behavior and hydrologic response of poorly lithified sediments. These considerations, and the variety of observations and models proposed, highlight the importance of understanding the occurrence and micromechanisms of cataclasis in sediments.

In this study, we present evidence for cataclasis in immature, poorly lithified, Tertiary sediments naturally deformed under low confining pressures from the Sand Hill fault zone, Albuquerque Basin, and from individual deformation bands within similar Tertiary sediments in the Socorro Basin. Both basins are within the Rio Grande rift, New Mexico, USA. Microstructural observations with optical, back-scattered electron (BSE) and secondary electron (SE) microscopy indicate that the mechanism of grain breakage varies with mineralogy and relative strength. PSD measurements indicate a greater proportion of large grains in the faulted sediments than predicted by the constrained comminution model. We interpret these observations and PSD data as the result of deformation under low confining pressures and posit that this is an explicit example of controlled particulate flow, as it appears that the amount of grain boundary sliding is more than would be required by or dependent on the fracturing of grains (Borradaile, 1981). These results have implications for the formation of macroscopic fault zone structures, interpretation of deformation history, fault zone diagenesis, and the impacts of normal faults in sediments on subsurface fluid flow.

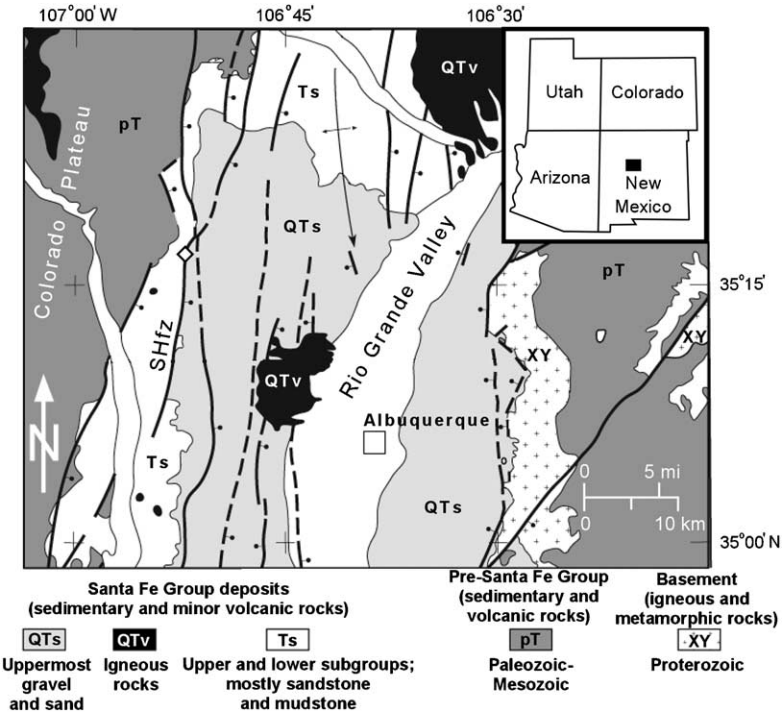

Fig. 1. Study site (open diamond) along Sand Hill fault zone (SHfz) in Albuquerque basin of Rio Grande rift. Inset shows regional location. Faults are generalized; not all faults are shown. Modified from Hawley et al. (1995) and Hawley (1996) by S. Connell. The second site is south of the map area shown (cf. Herrin, 2001).

2. Geologic setting and study areas

2.1. Sand Hill fault site

The Sand Hill fault is one of the major normal faults bounding the Rio Grande rift, and marks the western margin of the Albuquerque basin (Hawley et al., 1995; Fig. 1). It is a growth fault juxtaposing synrift sediments of the Pliocene–Pleistocene upper Santa Fe Group against middle Miocene to Oligocene sediments of the lower and middle Santa Fe Group. Based on outcrop observations and geophysical and borehole geological data, displacement increases from ~10 to ~600 m downdip (Hawley et al., 1995; Heynekamp et al., 1999). The lower Santa Fe Group sediments are dominantly fine-grained sand, with subordinate medium-grained sand, silty sand, and mud. These sediments were deposited in dune, fluvial, and mixed playa and dune environments. The upper Santa Fe Group sediments are largely fluvial, with minor aeolian deposits, and include sand, silt, and mud, locally capped by gravel (Tedford and Barghoorn, 1999). In the area sampled, the sediments cut by the fault are lithic arkoses and feldspathic litharenites (Beckner and Mozley, 1998; Fig. 2). Most of the lithic fragments (70–90%) are volcanic rock fragments. Excepting zones of calcite cementation (Mozley and Goodwin, 1995), all of the materials in the fault zone are friable and easily disaggregated. Stratigraphic constraints (Connell et al., 1999; Tedford and Barghoorn, 1999; S. Connell, written commun., 2001) and vitrinite reflectance data (William Shea, personal commun., 1998) suggest that current exposures of the Sand Hill fault were never buried more than 1 km. This limits overburden pressure during deformation to 20–30 MPa.

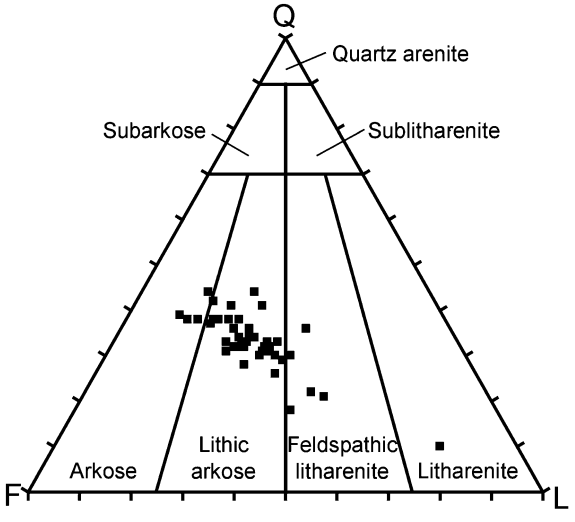

Fig. 2. Ternary diagram showing the relative proportions of quartz (Q), feldspar + granitic/gneissic fragments (F) and lithic fragments (L) in thin sections of sediments from the footwall of the Sand Hill fault at the study site. Data from Beckner (1996). Sandstone classification from Folk (1974).

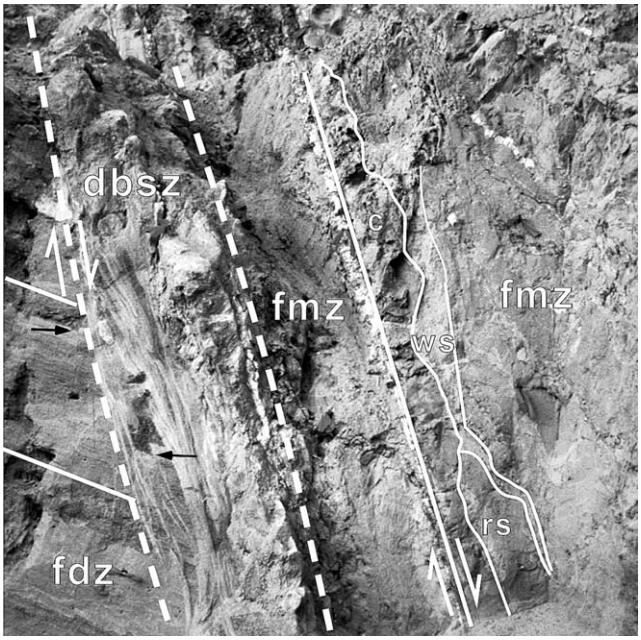

Fig. 3. Shear zone of coalesced deformation bands (DBSZ, outlined by dashed lines) forming contact between footwall damage zone (fdz) and footwall mixed zone (fmz) within Sand Hill fault zone. Viewed to the north. Core zone and main slip surface of fault are right of the fmz (east). Offset is at least several meters. Solid lines delineate tilted bedding in fdz and clay-rich (c), white sand (ws), and red sand (rs) beds transposed into foliation in fmz. Black arrows indicate offset of coarse-grained layer across part of DBSZ (see text). Width of photo is 3 m.

2.2. Fault zone structures

Fractures are the basic structural unit of faults in crystalline or lithified, low porosity sedimentary rocks. The internal structure of these faults can be subdivided into three architectural elements representing a progressive increase in deformation intensity and slip localization: protolith, damage zone, and core (Caine et al., 1996). Faults in lithified, high porosity sandstones have deformation bands (narrow, tabular zones of displacement, compaction, and/or cataclasis) as the basic structural unit and eventually develop discrete, macroscopic slip surfaces, which are effectively fractures with regard to fluid flow (Aydin, 1978; Aydin and Johnson, 1978; Underhill and Woodcock, 1987; Antonellini et al., 1994; Antonellini and Aydin, 1995). Faults in poorly lithified sands can also have deformation bands as the basic structural unit but do not contain macroscopic fractures (Heynekamp et al., 1999; Sigda et al., 1999; Rawling et al., 2001). Where displacement is greater than the local mean bed thickness, large-displacement normal faults in poorly lithified sediments, exemplified by the Sand Hill fault, typically have an additional architectural element, the mixed zone, between the damage and core zones (Mozley and Goodwin, 1995; Heynekamp et al., 1999; Rawling et al., 2001; Figs. 3 and 4). Mixed zones are compositionally and structurally heterogeneous. The degree of deformation may range from rotated but intact bedding, to bedding transposed into foliation, to penetrative deformation in the form of sediment disaggregation and

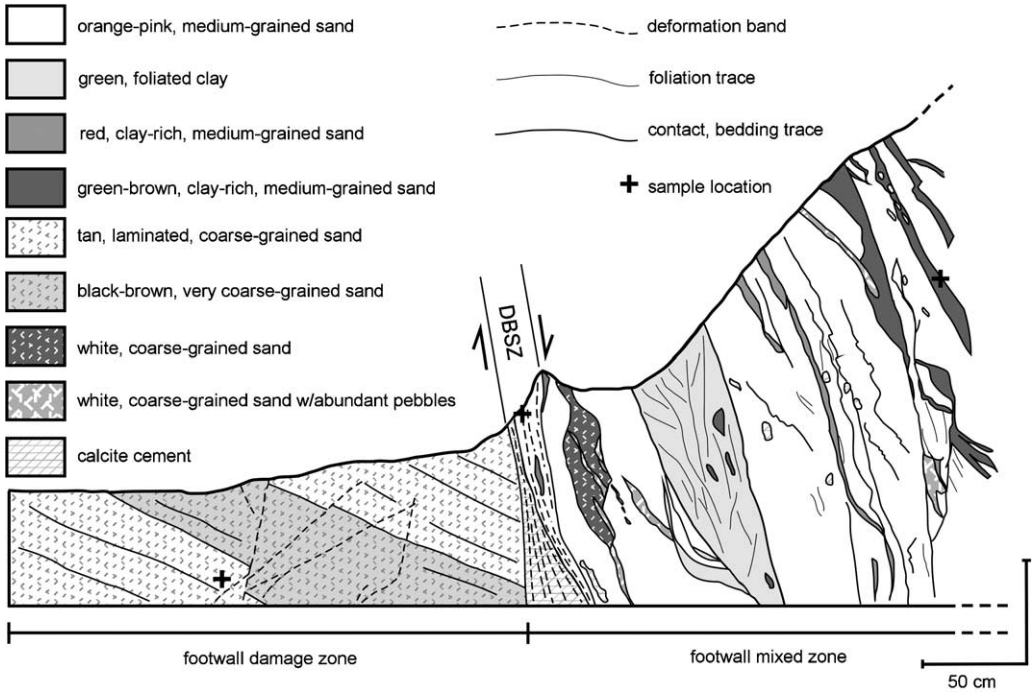

Fig. 4. Map of excavated outcrop in footwall of Sand Hill fault zone. Viewed to the north. Fault core is beyond right (east) side of excavation. Crosses show locations of one of each of the protolith (sediment from damage zone), mixed zone, and DBSZ samples. Complex mixed zone relationships largely represent sedimentary layers transposed into fault-parallel compositional foliations, with local development of shear zones and intense sediment mixing along relict sedimentary contacts.

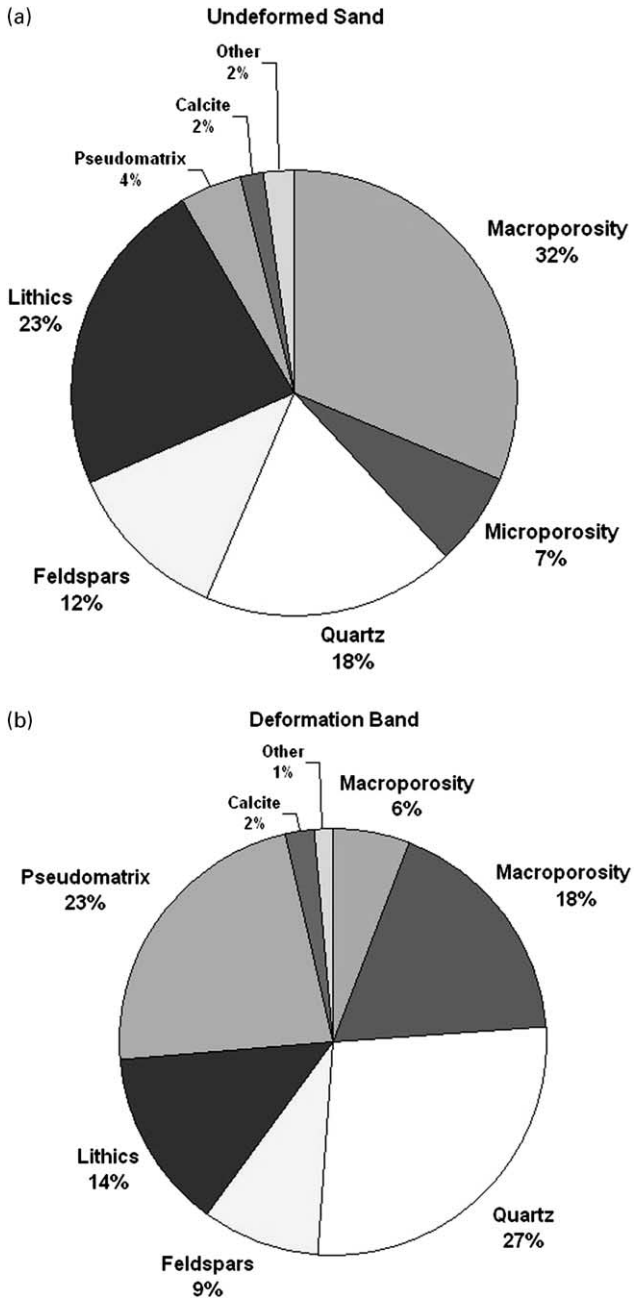

Fig. 5. Compositional data from the Bosque del Apache site. (a) Average of five point counts of the host sand. (b) Average of five point counts of the deformation band shear zone. Data from Herrin (2001). Pseudomatrix is clay-sized matrix produced by mechanical processes.

mixing at the grain scale, all within the range of a meter or less. Commonly the boundary between the mixed zone and protolith is a shear zone of coalesced deformation bands (deformation band shear zone, hereafter referred to as DBSZ). These shear zones represent strain localization (Fig. 3) and concentrated cataclasis. In general, it is not possible to estimate the amount of strain in the mixed zone, as offset on the fault is too great. However, a lower bound on the shear strain in the DBSZ of $\gamma = 7$ to 11 at the Sand Hill fault site is obtained from the offset of a sliver of coarse-grained sediment (Fig. 3).

2.3. Bosque del Apache site

The second study site is at the southern margin of the Socorro basin in central New Mexico, approximately 160 km south of the Sand Hill fault site. It is a railroad cut within the Bosque del Apache National Wildlife Refuge in which are exposed sand, gravel, and conglomerate beds of the Popatosa Formation of the Lower Santa Fe Group (Herrin, 2001). The sands and gravels represent alluvial fan, transitional fan, and eolian facies. Compositional data for the undeformed and deformed sands are given in Fig. 5. Although the gravel beds are moderately indurated, the sands are poorly lithified and easily excavated with hand tools. The outcrop is 135 m long and is cut by numerous DBSZs and two faults with slip surfaces, all of which strike northwest–southeast and have normal slip sense (Herrin, 2001). Structures dip both northeast and southwest. Maximum burial is not well constrained, but stratigraphic considerations suggest it is no greater than at the Sand Hill fault site, with similarly low confining pressures during deformation. The DBSZ studied is 10 cm wide and has a throw of ~3 m, resulting in a shear strain of $\gamma = 30$ in the DBSZ.

3. Microstructural analysis

3.1. Sample collection

We collected two sediment samples each from the protolith (undeformed material within the damage zone), mixed zone, and DBSZ for PSD measurements from the footwall of the Sand Hill fault. Three of the samples were collected from the outcrop shown in Fig. 3. The mixed zone and DBSZ regions sampled do not represent deformed equivalents of the adjacent protolith sediment; displacement on the fault is too great to track individual beds into the fault zone. At the Bosque del Apache study site an isolated DBSZ cutting a thick sand layer and the host sand were sampled, allowing direct comparison of a deformed sand with its protolith.

The samples were collected by gently excavating a small hole in the outcrop with a paint scraper and brushing ~3 cm^3 of loose sediment into a plastic container. In most cases, excavation and subsequent mild shaking of the sediment were sufficient to completely disaggregate the sample. We also collected multiple hand samples from all parts of the fault zone at the Sand Hill fault site for petrographic analysis by drilling into the outcrop with a hole saw and surrounding the sediment core with expanding insulation foam (method by Chris Dimeo, personal commun., 1997).

3.2. Microscopy

Thin sections were made from Sand Hill fault samples impregnated with low viscosity epoxy; however, the samples were extremely fragile and friable and plucking is a problem in thin-section preparation. This precludes PSD

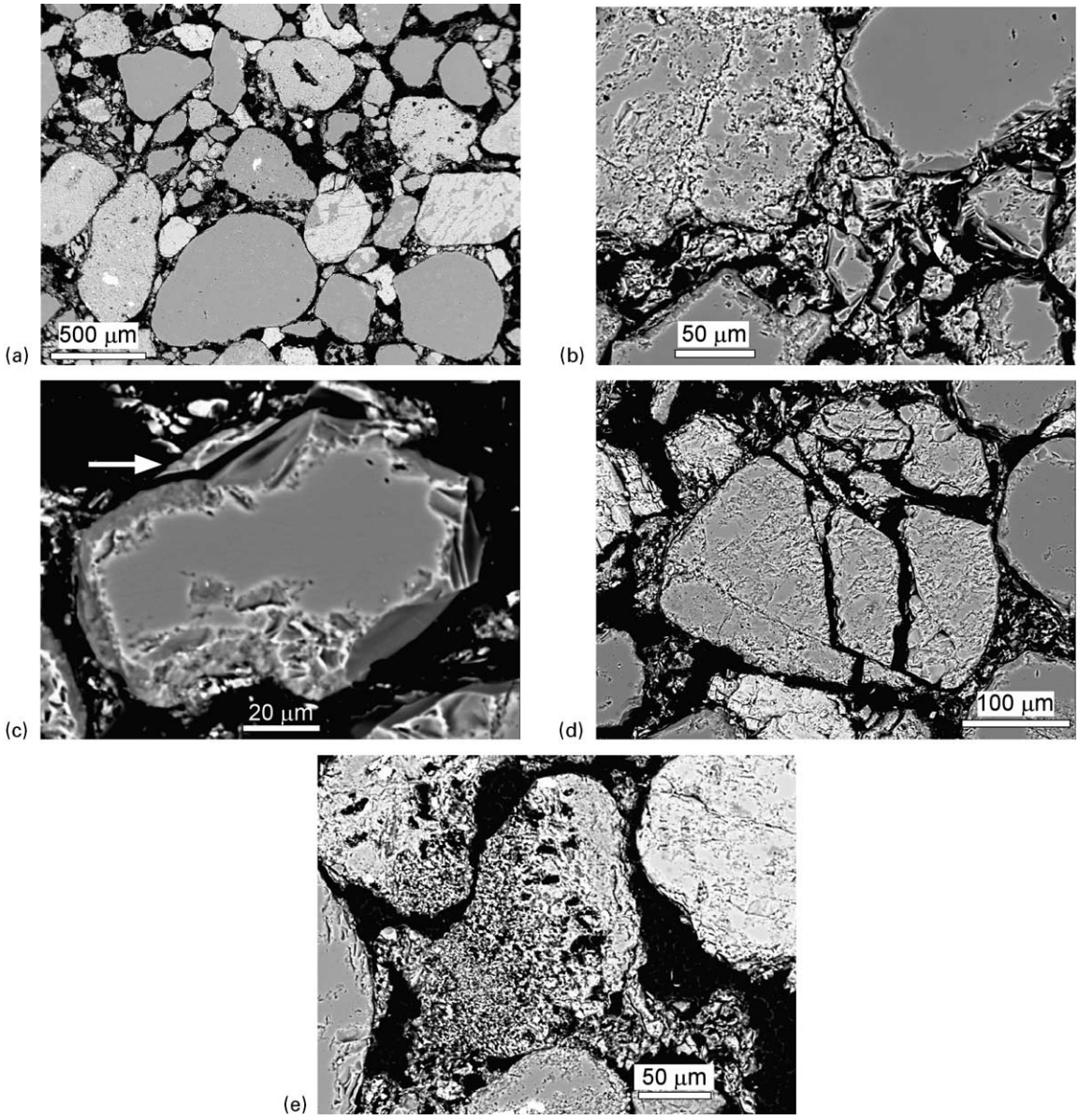

Fig. 6. Back-scattered electron images from DBSZ at Sand Hill fault site. (a) Typical texture evident in thin section. Note large, rounded relict grains touching each other and scarcity of transgranular fractures. Quartz is dark gray and smooth; feldspar and lithic fragments are light gray and rough. Large black spaces are gaps left by plucked grains. (b) Close-up of fine-grained material from DBSZ. Note conchoidal fractures on quartz grain margins and fine quartz flakes mixed with feldspar and clay(?) between sand grains. (c) Quartz; approximately 50% of margin is composed of fresh, smooth conchoidal fracture surfaces. Note the elongate, sharp flake immediately adjacent to matching fracture surface (arrow). (d) Feldspar broken by transgranular fractures. (e) Apparently ductile deformation of a volcanic lithic fragment, probably by distributed microcracking and/or deformation following alteration.

measurements within the thin sections. We examined the thin sections with optical and back-scattered electron (BSE) microscopy. We also examined loose grains from subsets of several of the Sand Hill fault PSD samples to characterize grain-surface morphology. The grains were boiled for 10 min in concentrated HCl, rinsed with water and acetone, and air-dried. They were then mounted on double-sided tape on stubs, carbon-coated, and observed with a Cameca SX-100 electron microprobe in secondary electron mode (SEM). Several dozen grains were examined from each sample, which is a sufficient number to address the variability in the samples (Krinsley and Doornkamp, 1973). We did not make thin sections or grain mounts of the Bosque del Apache samples. However, previous studies indicate that the sands and DBSZs at this site are compositionally, petrographically, and microstructurally similar to the sands at the Sand Hill fault study site (Sigda et al., 1999; Herrin, 2001).

In BSE images of thin sections, mixed zone and DBSZ samples typically exhibit rounded relict grains, with interstices filled by smaller, more angular grains, fine grained comminution debris, agglomerations of clay-size particles

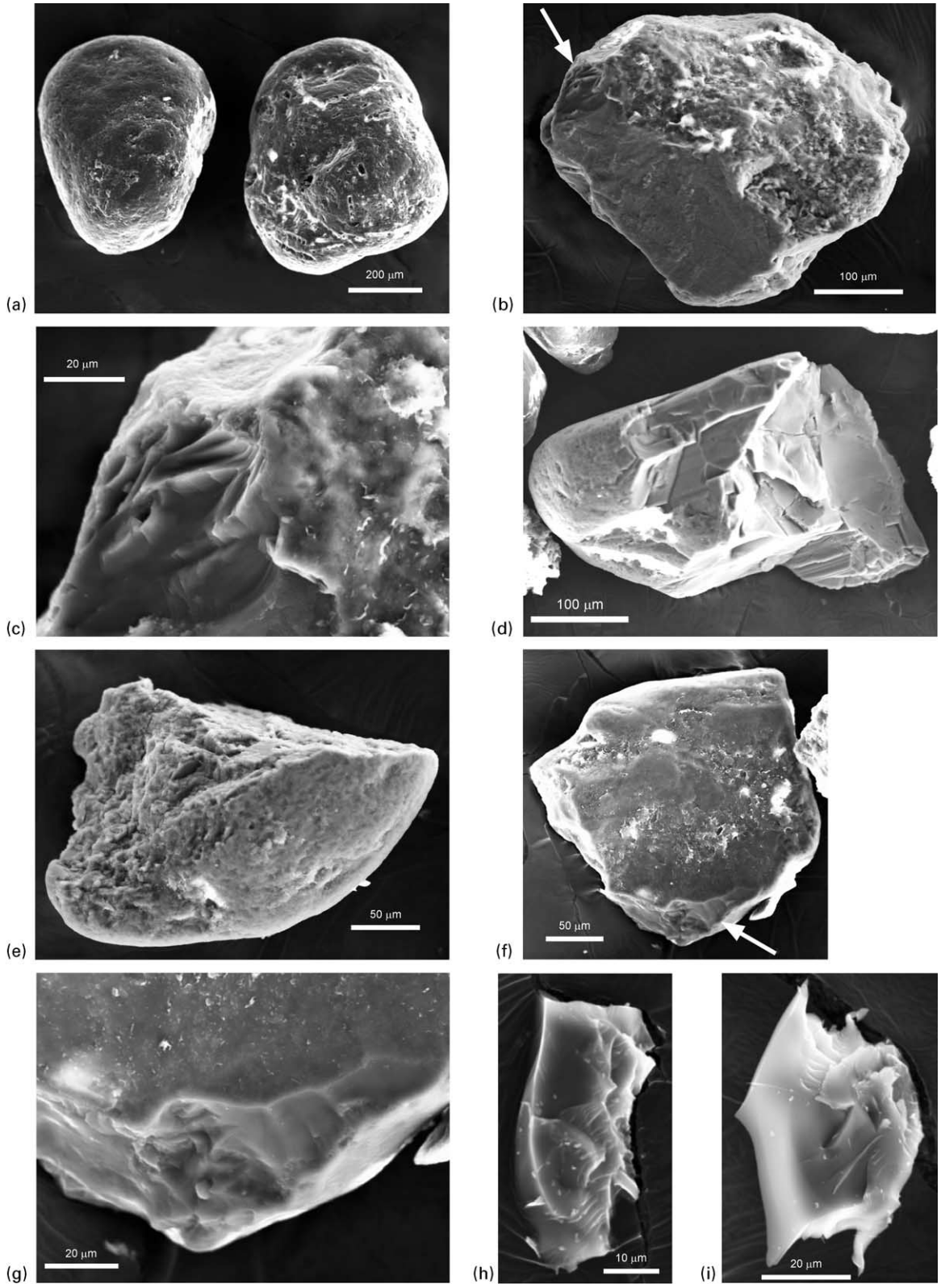

Fig. 7. Secondary electron images: (a) Undeformed quartz and lithic grains from protolith. (b) Area of fresh conchoidal fracture (arrow) on quartz from mixed zone. Remainder of grain surface may consist of older fracture surfaces covered with diagenetic coatings. (c) Close-up of region indicated by arrow in (b). Note smooth, curving fracture surfaces, compared with other coated areas. (d) Broken feldspar from DBSZ. (e) Broken lithic fragment from DBSZ. (f) Area of fresh conchoidal fracture (arrow) on quartz from DBSZ. (g) Close-up of region indicated by arrow in (f). Note small (cleavage?) flakes on remainder of grain surface. (h) and (i) Quartz fracture flakes from DBSZ. Flakes are completely bounded by fresh, smooth, often ribbed conchoidal fractures, and have delicate protrusions.

and irregular blebs of calcite (Fig. 6a). The large grains commonly touch and generally are not isolated from their neighbors by finer-grained matrix. Transgranular fractures are rare. At higher magnifications it is apparent that much of the comminution debris is composed of small quartz fragments (Fig. 6b). The most striking observation is that many of the quartz grains have ragged perimeters with fresh conchoidal fracture surfaces (Fig. 6b and c). Fig. 6c shows a typical example of a quartz grain with fresh conchoidal fractures around ~50% of its margin and rougher, but less angular, surface textures around the remainder. The matching of elongate, sharp flakes to adjacent fresh fractures is quite common. Occasionally flakes are seen still partially attached to the host grain. Conspicuous by their scarcity are transgranular fractures that shatter grains into highly angular fragments, and large numbers of blocky or tabular fragments bound by smooth, curved surfaces that would be the product of such fracturing. These more 'typical' cataclastic textures have been observed in naturally deformed sands and sandstones (e.g. Lucas and Moore, 1986; Antonellini et al., 1994), and have been created in experimentally deformed sand and sandstone (e.g. Borg et al., 1960; Marone and Scholz, 1989; Menéndez et al., 1996). Most of the transgranular fractures in samples from the Sand Hill fault were observed in feldspars (Fig. 6d) and volcanic lithic grains. Volcanic lithic grains also commonly deform by distributed deformation, which may be distributed microcracking of the fine-grained matrix of the grain (cf. Herrin, 2001) and/or deformation following alteration to minerals such as clays (Fig. 6e).

SEM imaging of individual particles allows examination of the morphology of the particle's surface, and there is a large literature on the subject (see Krinsley and Marshall (1987) for a review). However, it has the disadvantage of not preserving spatial relationships amongst the particles as in BSE imaging of thin sections (e.g. Fig. 6a and c). We examined grains from the protolith, mixed zone and DBSZ. Protolith grains (Fig. 7a) are well rounded and have surface textures such as v-shaped mechanical indentations, small upturned cleavage plates, and precipitated surface coatings indicative of their sedimentary and diagenetic history (cf. Krinsley and Doornkamp, 1973). We observed no evidence of tectonic deformation, such as fresh fracture surfaces or small fracture bounded particles (see below). Undeformed sand grains from the mixed zone and DBSZ are similar in appearance to protolith grains.

Many grains from the mixed zone show evidence of flaking along their edges. Fig. 7b and c shows a small area of fresh conchoidal fracture on an irregular quartz grain. The remainder of the grain surface may be older fractures covered with diagenetic coatings. Compared with the DBSZ sample, cleavage fragments and flakes are rare.

The majority of the grains from the DBSZ show shapes and surface textures indicative of cataclasis, consistent with optical and BSE observations in thin section. The differing modes of fracture of feldspars (largely transgranular fracturing), lithic fragments (alteration and/or crushing to fine particles and transgranular fracturing), and quartz (flaking of edges) are evident. Broken feldspars (Fig. 7d) appear to be the products of transgranular fracturing of detrital grains. Rounded edges with relict sedimentary textures are visible adjacent to jagged edges composed of large, clean, fracture surfaces. The fractures in feldspar are largely cleavage-controlled. Fig. 7e shows a lithic fragment with a similar overall morphology to the feldspar in Fig. 7d, but it is uncertain whether this grain deformed by transgranular fracturing or 'crushing' and generation of fine particles (cf. Fig. 6e).

Fig. 7f and g shows irregular quartz grains partly bounded by fresh, smooth, conchoidal fracture surfaces. The remainder of the surface textures appear similar to those of the protolith grains. Quartz fracture flakes are abundant in the DBSZ sample (Fig. 7h and i). They have smooth, conchoidal fracture surfaces and often extremely sharp, delicate edges. These flakes are the disaggregated equivalents of the flakes observed in thin section (e.g. Fig. 6b and c), and most have dimensions on the order of 20–30 μm.

4. Particle size distributions

4.1. Particle size measurement

We measured particle size distributions with Scion Image image analysis software interfaced with a video camera attached to a petrographic microscope. A small portion of the sediment sample was scattered onto a glass slide and the slide was traversed until 30 or 60 non-overlapping images of the disaggregated grains were collected. A magnification of 4× was used, which provides a resolution (smallest resolvable particle size) of 0.0064 mm and a large enough depth of field that all visible particles were in sharp focus for accurate digitization. The largest particles observed were 0.5–0.7 mm in diameter for all datasets, resulting in an observable size range of three orders of magnitude. This size range is the same as that considered by Blenkinsop (1991). Typically, several hundred grains were visible in each image, and no particles larger than the field of view were encountered. The grayscale images were converted to pure black (grains) and white (background) images and touching grains were separated manually in each image. We calculated the nominal section diameter and corrected count for each grain. The nominal section diameter is the diameter of a circle equal in area to the area of the grain in the plane of its largest and intermediate diameters (Mazzulo and Kennedy, 1985) and is calculated based on the digitized projected area of the grain. This method gives a direct estimate of the size of the grain in three-dimensional space, because the images are projections of the grains, not slices through them (as in a thin section). The corrected count accounts for the fact that large grains are more likely to intersect the edge of the image, and thus their area cannot be determined, and they cannot be counted. This would

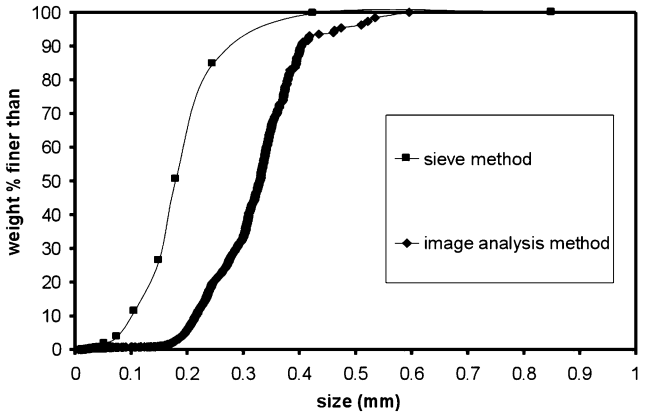

Fig. 8. Crushed quartz sand PSDs by weight determined by sieving and image analysis methods. Image analysis distribution by number was converted to distribution by weight by calculating equivalent spherical sizes from nominal section diameters and assuming a density for all particles of 2.65 g/cm^3.

result in the larger grains being underrepresented in the PSD. The corrected count of each grain is defined as

$$\frac{W_X W_Y}{(W_X - F_X)(W_Y - F_Y)} \quad (1)$$

where W_X and W_Y are the image widths and F_X and F_Y are the maximum grain dimensions, or 'caliper dimensions' in the X and Y directions, respectively (Russ, 1991, 1999; pp. 529–532). Thus the count of each grain is a real number (say, 1.15), not the integer 1, and the corrected count increases with grain size. In this study, we found that using either corrected or uncorrected counts has little effect on the resulting PSDs or the fitted models.

The raw data of calibrated grain sizes and corrected counts were saved as a text file and cumulative particle size distributions were calculated. Consistent with previous workers (Sammis et al., 1987; Marone and Scholz, 1989), we estimated counting errors by assuming the data were selected from a Poisson spatial distribution of particles (Wilson, 1952). The data are presented as cumulative distributions in log(number)–log(size) space. This follows directly from the definition of a fractal set:

$$N = \frac{C}{r^D} \quad (2)$$

where N is the number of objects with a characteristic linear dimension greater than r, C is a constant, and D is the fractal dimension (Turcotte and Huang, 1995). We used a weighted, least-squares routine to fit a power law model to the linear regions of the data sets. The weights are based on the standard deviation of the measurements, thus giving greater weight to data points representing more counts.

To check the precision and accuracy of this method, we measured the PSD of a sample of crushed quartz sand by both our image analysis method and traditional sieving techniques. Unless the particles are perfect spheres, accuracy is extremely difficult to determine or even define for PSD measurements, as different size measurement techniques measure different size and/or shape attributes of the particles and all report particle size as some convolution of size and shape (Kennedy and Mazzulo, 1991; McCave and Syvitski, 1991). Differences between techniques increase with increasing irregularity (e.g. angularity) in particle shape. To a first approximation, sieving yields particle size as the intermediate axis of the particle, whereas projected images of grains on a slide include the intermediate and long axes of the particles, and the derived nominal sectional diameter is probably a closer measure of the 'true' particle size (Mazzulo and Kennedy, 1985). Thus, for a given particle, sieving yields a smaller size estimate than the nominal section diameter determined from image analysis. Of greater importance is whether a given technique reproduces the true shape of the PSD being investigated, e.g. the number of modes, the skewness, etc. PSDs determined by sieving are by weight, i.e. they report the distribution of particle sizes as a function of the weight of the particles in each size class. To compare our two datasets, we converted the PSDs by number from the image analysis method to PSDs by weight by calculating an equivalent spherical weight for each measured grain. This was done by calculating the volume of a sphere with the same diameter as the nominal section diameter, and assuming a grain density of 2.65 g/cm^3.

The shape (as defined above) of the PSD of the crushed quartz sand determined by image analysis closely matched that determined from sieving and, as would be expected from the above discussion, was offset to larger particle sizes by ~150 μm (Fig. 8). This offset is larger than that observed by Mazzulo and Kennedy (1985) in a similar comparison, but the crushed quartz particles in our test were highly angular whereas Mazzulo and Kennedy (1985) studied well rounded beach sands. We conclude that the imaging technique provides a sufficiently accurate and precise measure of the PSD over the size range investigated (0.006– ~ 1 mm). Its advantages are that minimal sample preparation is required, very small samples can be easily measured, thousands of grains can be quickly counted, and the derived nominal section diameters of individual grains are probably a better measure of the true particle size.

4.2. Sand Hill fault samples

The protolith samples (Fig. 9a and b) are characterized by PSDs with kinks at intermediate grain sizes. These data are consistent with field estimates of the relative particle size distributions of the two samples. The PSDs of both mixed zone samples (Fig. 9c and d) show more subdued 'bumps'. In contrast, the PSDs of DBSZ samples are largely linear with tails at the smallest and largest grain sizes. Qualitatively, the progression from undeformed protolith to DBSZ involves a flattening of the PSD to a power law trend and a relative decrease in the number of intermediate sized

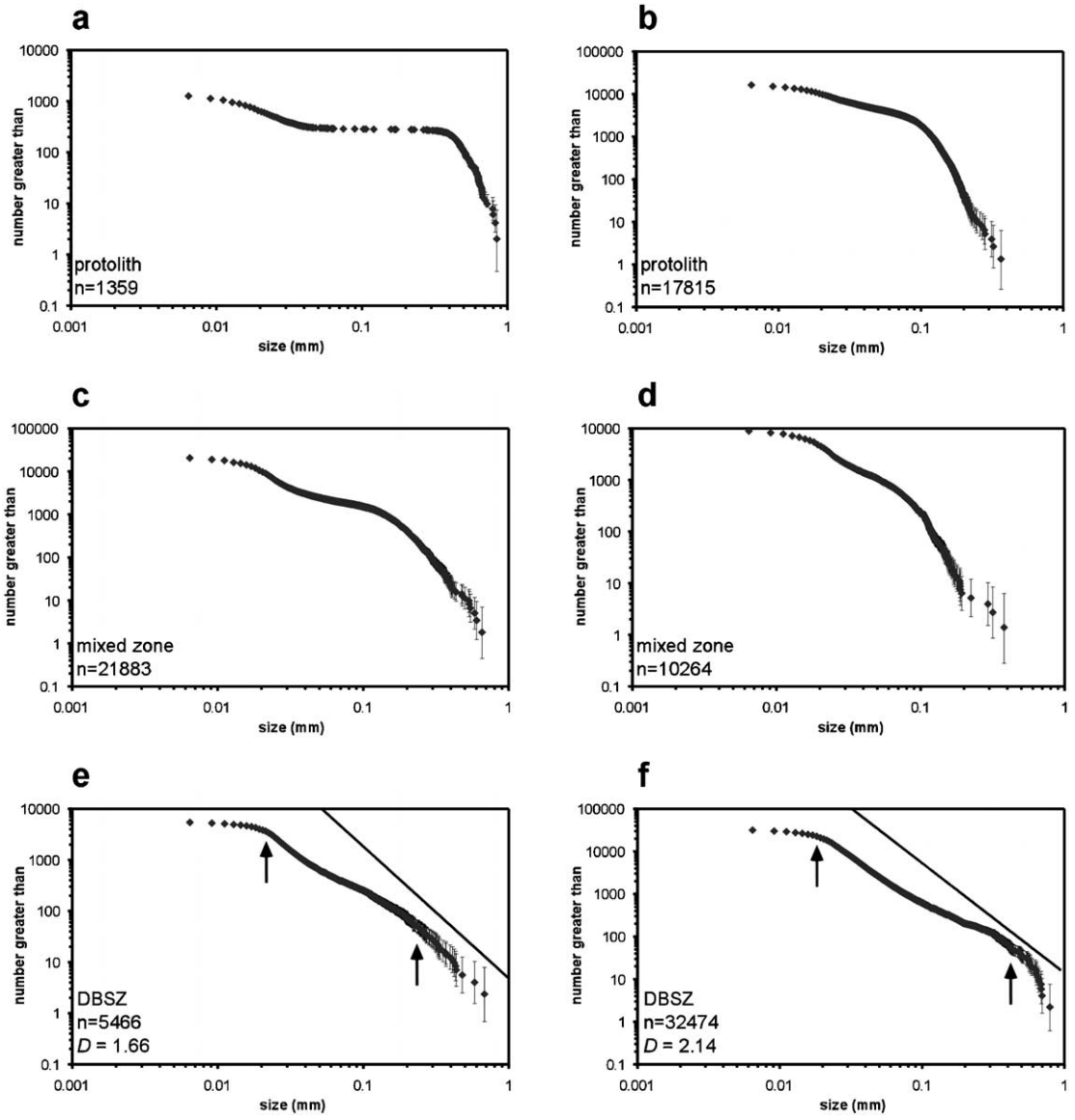

Fig. 9. Sand Hill fault PSD data. Numbers of particles measured are indicated on each plot: (a), (b) protolith; (c), (d) mixed zone; (e), (f) DBSZ samples. *D* values from power law models are given. Dashed reference lines have slopes (*D* values) equal to 2.6.

particles. This progression is consistent with the field interpretation that the DBSZ has undergone more intense, localized deformation than the mixed zone.

By the chi-squared goodness-of-fit test, a power law model adequately describes the PSD of both of the DBSZ samples (Fig. 9e and f and Table 1). Although in both cases an acceptable fit can be made to the entire range of data, we have only used the most linear portion, bounded by the arrows in Fig. 9e and f, in fitting the models. In terms of a fractal model, the points identified by the arrows are interpreted as the lower and upper fractal limits (cf. Blenkinsop, 1991). The fitting parameters for these models and the resulting *D* values (power law exponents) are shown in Table 1. These *D* values are three-dimensional fractal dimensions because, as noted above, the particle sizes are nominal sectional diameters determined from projected areas of grains. The three-dimensional *D* values are 1.66 and 2.14 (Table 1), and indicate a greater proportion of large particles in the PSD than predicted by the constrained comminution model of Sammis et al. (1987; D ~ 2.6).

Table 1
Deformation band shear zone particle size distribution data

Sample locality	n[a]	D[b]	$\chi^2 \leq \chi^2_{crit}$ ($\alpha = 0.01$[c])
Sand Hill fault	5466	1.66	$4.6 < 404$
Sand Hill fault	32474	2.14	$15.7 < 664$
Bosque del Apache	22729	2.07	$20.5 < 434$

[a] Number of particles measured.
[b] Power law exponent (3-D fractal dimension).
[c] Chi^2 goodness-of-fit test results at 99% confidence level.

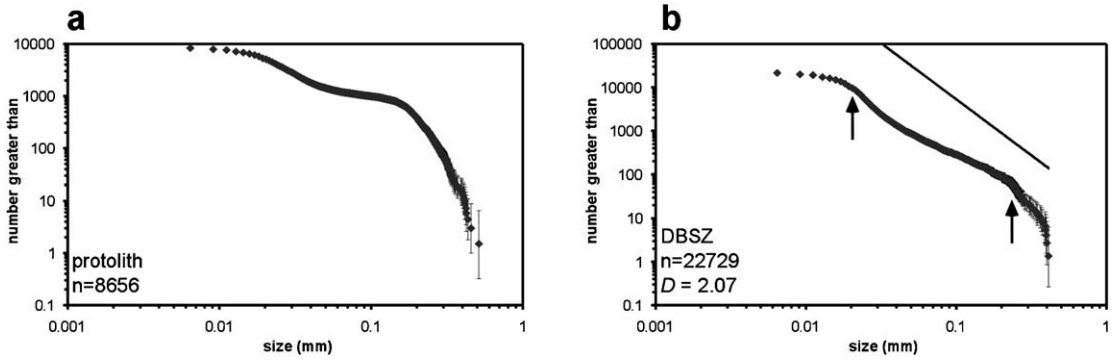

Fig. 10. Bosque del Apache PSD data. Numbers of particles measured are indicated on each plot: (a) protolith (compare with Fig. 9a and b); (b) DBSZ (compare with Fig. 9e and f). D value from power law models is given. Dashed reference line has slope (D value) equal to 2.6.

4.3. Bosque del Apache samples

The PSDs of DBSZ material and its host sand at the Bosque del Apache site allow a direct comparison of a deformed sand with its protolith. Qualitatively, the undeformed and deformed sands show similar PSDs to the analogous Sand Hill fault materials (Fig. 10a and b). The DBSZ data can be fit with a power law model over its entire range; however, we have only fit a model between lower and upper fractal limits as indicated (Fig. 10b). The resulting three-dimensional D value is 2.07 (Table 1).

5. Discussion

5.1. Mechanisms of cataclasis

The constrained comminution model of Sammis et al. (1987) predicts that when two particles of equal size come into contact, one will deform by transgranular fracture. Ultimately, this results in a characteristic microstructure in which large relict grains are surrounded by a finer grained matrix, and in general, no two grains of equal size are touching. This has been observed in natural (e.g. fig. 5a in Blenkinsop, 1991) and artificial (e.g. fig. 8a and b in Marone and Scholz, 1989) fault gouges. However, we observe in thin section that: (1) relict grains in our samples are relatively abundant and commonly are in contact (Fig. 6a); and (2) transgranular fractures are relatively uncommon and appear to be mineralogy dependent. These facts, together with the observations of ragged edges on quartz grains, associated small quartz flakes, distributed deformation of lithic grains, progressive flattening of the PSDs, and the low D values of the DBSZ PSDs imply that the mechanism of cataclasis that we observe is not constrained comminution *sensu stricto*, as defined by Sammis et al. (1987).

Our low D values, ~1.7–2.1, compared with the value of 2.6 predicted by the model of Sammis et al. (1987), indicate that for a given number of large particles, there are fewer intermediate and small particles in deformed poorly lithified sediments (compare the PSDs with the reference lines in Figs. 9e and f and 10b). The progressive flattening of the PSDs to a power law with increased deformation in both the Sand Hill fault and Bosque del Apache samples indicates that cataclasis preferentially removed the intermediate size particles. Many of the quartz flakes and conchoidal fracture surfaces on quartz grains have dimensions of roughly 20–40 μm (Figs. 6b and c and 7b and g–i). If this is generally the case, then flaking of these small fragments of approximately constant size from grain margins will more efficiently break down the intermediate size particles in the PSD than the largest particles. Also note that this size range, 20–40 μm, corresponds roughly to the upper 'tail', of all three DBSZ PSDs (Figs. 9e and f and 10b). This may indicate that particles in this size range are the smallest that are produced in abundance during cataclasis, and that once produced, these fragments do not break down further.

Why are the modes of grain fracture and the associated D values of the resulting PSDs different from the predictions of the constrained comminution model of Sammis et al. (1987)? Marone and Scholz (1989) conducted shear experiments on Ottawa sand at 20 MPa confining pressure to $\gamma = 2.3$. They observed fewer transgranular fractures in particles of all sizes and more spalling or flaking of grains than in experiments conducted at 100 MPa. The ragged grain boundaries on the larger particles and many quartz flakes in their photomicrographs (fig. 9d and e of Marone and Scholz, 1989) are similar to the quartz textures from the Sand Hill fault zone. Many of the smallest, most elongate flakes are comparable in size with those in this study. The D value they determined was 2.40, slightly less than the value for constrained comminution. These results suggest that low confining pressures promote the spalling and flaking of quartz, as we observe, as opposed to transgranular fracturing.

It is important to note that our D values are lower than those of Marone and Scholz (1989). There are several possible explanations and/or potential factors contributing to this. The grains imaged by Sammis et al. (1987) and Blenkinsop (1991) are much more angular than those in this study. This may be expected in gouges derived from intact igneous and metamorphic rocks as opposed to our samples, which are

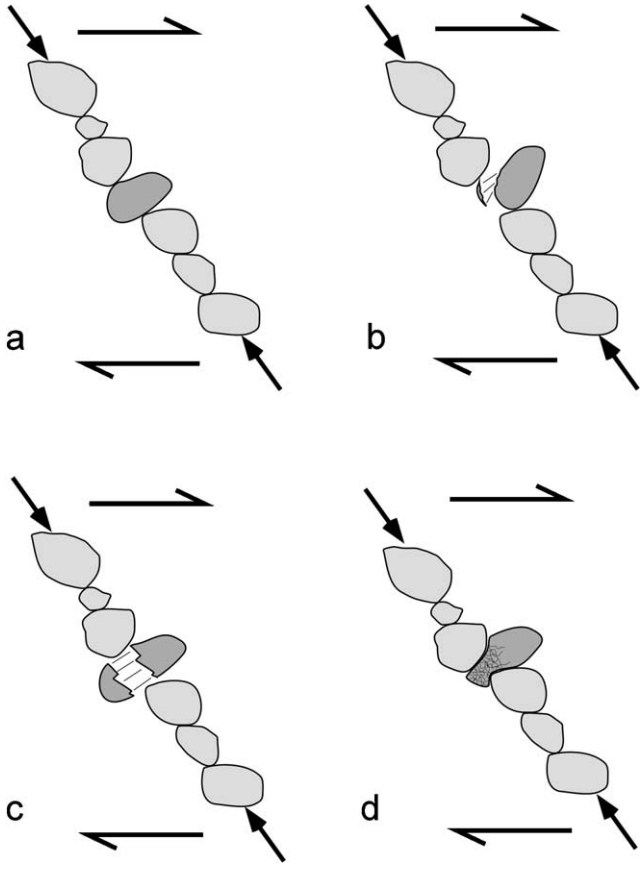

Fig. 11. Grain bridge model for deformation within the Sand Hill fault zone. (a) Grains aligned coaxial to applied stress (arrows) offer resistance to shear within deforming zone. Concept after Biegel et al. (1989) and Hooke and Iverson (1995). Grain bridges may fail by (b) flaking or spalling of quartz, (c) transgranular fracturing of feldspar or lithic fragments, or (d) distributed microcracking of lithic fragments.

derived from rounded sedimentary grains in poorly lithified, immature sediments. The proportion of available grains that are actively being flaked or crushed, and the number of flakes removed from each grain may vary. This may be because much of the deformation in our samples was accommodated by grain boundary sliding during controlled particulate flow. This possibility is explored further below.

The mineralogy and composition of the protolith sediments are important variables. Marone and Scholz (1989) deformed a starting material of nearly pure quartz sand, whereas our protolith materials have substantially less quartz (Figs. 2 and 5a). Fig. 5 shows the composition of material from a DBSZ and an adjacent undeformed sand at the Bosque del Apache site. The subtotal of framework grains (quartz + feldspar + lithic fragments) changes little from the undeformed sand (53%) to the DBSZ (50%). However, the relative proportion of quartz in this subtotal increases from 34% in the undeformed sand to 54% in the DBSZ. This is consistent with flaking of small chips off the margins of quartz grains being less efficient than wholesale fracturing at reducing the grain size. The decrease in percentage of lithic fragments and the increase in pseudomatrix suggests that many lithic fragments were crushed, a suggestion supported by BSE images (Herrin, 2001). In general, the compositional data in Fig. 5 are consistent with our microstructural observations from the Sand Hill fault zone. However, it appears possible that the D value of cataclastically deformed, poorly lithified sediments is sensitive to composition. This warrants a more systematic study.

It is also possible that our samples have not yet achieved a steady-state PSD and that with further deformation the PSDs would change, perhaps resulting in higher D values. We have no constraints on this possibility. However, we estimated the shear strain across the two DBSZs in this study at $\gamma = 7$ to 11 and 30, respectively, based on offset marker laminae. These values are much higher than the range of shear strains (0.1–2.88) attained by Marone and Scholz (1989), in which many of their artificial gouges had D values of approximately 2.6. We therefore conclude that the relative strengths of grains of different composition are a more important factor in determining D values in poorly lithified sands.

In sum, we believe that a scenario of cataclasis under low confining pressure, with a large component of grain boundary sliding, and the additional effect of compositionally dependent modes of grain fracture, can explain both our microstructural and textural observations and PSD data.

5.2. Deformation model

An explanation for the different modes of grain fracture exhibited by our samples is provided by the grain bridge model (Fig. 11). Mandl et al. (1977) observed via in-situ stress measurements that the state of stress in a deforming granular medium is highly heterogeneous. They attributed this to the formation and destruction of grain bridges coaxial with the applied maximum principal stress (Fig. 11). Resistance to shear in the granular medium is provided by compressive stress across the grain bridges. Biegel et al. (1989) hypothesized that failure of these grain bridges can be accomplished by slip along the boundaries of the shear zone, failure of asperities along the boundaries of the shear zone, intergranular slip between grains composing the bridge, or transgranular fracture of grains composing the bridge. A central tenet of the constrained comminution model is that, in most gouges, grain bridges fail dominantly by transgranular fracturing (Fig. 11c), eventually resulting in fractal PSDs with D values of 2.6.

The grain bridge model can also be applied to the deformed sediments of this study, with the mode of failure of the grain bridge dependent in part on the mineralogy and relative strength of the particles in the bridge (Fig. 11). Quartz grains fail by slip and associated abrasion or flaking (Fig. 11b). Volcanic lithic fragments fail by transgranular fracturing or pervasive microcracking (Fig. 11c and d), and feldspars fail by transgranular fracturing (Fig. 11c). We propose that these processes, in concert with a large component of grain bridge failure by grain slippage or slip along

shear zone boundaries (facilitated by low confining pressure), unaccompanied by cataclasis, can explain the lower *D* values we observe.

Strain accumulation in the Sand Hill fault zone occurred dominantly by particulate flow of disaggregated sediment. Field evidence for this deformation mechanism includes transposition of bedding into foliation, resulting in macroscopically ductile-appearing structures, and the tectonic mixing of disparate sediment types (Heynekamp et al., 1999). The microscopic observations and PSD measurements presented here indicate that grain fracture occurred, but the relative movements of most grains did not require intense intragranular deformation. Borradaile (1981) defined controlled particulate flow largely in terms of strain rate, for which we have no constraints. However, we suggest that the flaking or spalling type of grain fracture of quartz during cataclasis in the Sand Hill fault, together with the low *D* values in the PSDs, are evidence for controlled particulate flow. The strong quartz grains fractured only enough to facilitate easy slip between adjacent grains. Often grains were able to move past each other with no intragranular deformation at all. In this context, we interpret the extensive transgranular fracturing causing the failure of grain bridges and accumulation of strain in fault gouges from crystalline and lithified sedimentary rocks to be the product of dependent particulate flow. This is to say that, due to some combination of higher confining pressure, greater host rock stiffness, and the geometric constraints imposed by relatively rigid shear zone boundaries, grain size must be reduced by constrained comminution in the high-strain zone to allow continued localization of slip. In this situation, relative grain movements are dependent on grain fracture, which ultimately results in PSDs with *D* values of ~2.6. Conversely, in the poorly lithified sediments of this study, due to the low confining pressure, relatively less rigid shear zone boundaries due to the weak host sediments, and varied mineralogy, transgranular fracturing was largely a function of particle strength.

5.3. Implications

This study supports the observations of Lucas and Moore (1986) and Cashman and Cashman (2000) that cataclasis can occur during very low pressure deformation in poorly lithified and unlithified sediments. In our experience this has often been greeted with skepticism by structural geologists. However, as is apparent from our observations and those of the other studies summarized herein, there does not appear to be a simple, all-encompassing explanation for cataclasis in sediments and related materials. This warrants more detailed laboratory study of the development of PSDs, with particular emphasis on mechanical parameters that are difficult to constrain in the field, such as strain rate and fluid and confining pressure. Many important questions are unanswered. For example, based on ^{14}C dating of associated sediments, Cashman and Cashman (2000) suggested that the DBSZs in their study formed during seismic slip events. There are no such constraints in our study, and it is not known whether seismic slip rates are required for cataclasis in these materials.

Is it possible for the pre-lithification structures and cataclastic textures documented herein to be preserved if deformation continues after lithification? Post-lithification deformation likely would be in the form of discrete fractures, fracture networks, and relatively narrow zones of constrained comminution. It therefore seems probable that pre-lithification structures and textures can be preserved through protracted post-lithification deformation. They may be present in the matrix between these later structures. Examination of lithified samples from greater depth along the Sand Hill or similar faults, perhaps recovered from drill holes, could shed light on this issue. In addition, our observations suggest a direction for consideration of the relative timing of formation of deformation bands and diagenesis of currently well lithified sandstones (cf. Byrne, 1994). Deformation bands that contain evidence for extensive transgranular fracture of quartz must have formed under higher confining pressure. Quartz grains deformed dominantly by flaking at the edges record deformation at lower confining pressure in a poorly lithified state, followed by lithification.

Cataclasis in unlithified sediment may significantly impact subsequent diagenetic processes. Particle size reduction due to cataclasis may induce preferential cementation of the fault relative to the surrounding sediments due to the more reactive fine-grained comminution products and/or membrane effects during cross-fault flow (e.g. Whitworth et al., 1999).

An understanding of the nature of cataclasis in the unlithified sediments examined here is of considerable practical interest. The grain scale deformation mechanisms described herein produce the macroscopic structures observed in the field. Isolated cataclastic DBSZs in poorly lithified sediments have been shown to have two to three orders of magnitude lower permeability than their host sands, due to significant reduction of pore and grain size (Sigda et al., 1999). In larger faults, such as the Sand Hill fault, the macroscopic fault-zone structures and their arrangement into architectural elements result in hydrologic properties of the fault zone as a whole that are distinctly different from brittle faults in crystalline and lithified sedimentary rocks (Rawling et al., 2001). For example, the mixed zone is an architectural element with physical and hydrologic properties which are the result of controlled particulate flow of sediment under low stress conditions. Thus, the deformation mechanisms operative during faulting, themselves the result of the interaction between protolith material properties, strain rate and confining pressure, etc., define the resulting hydrologic impact of the fault within regional groundwater flow systems. In petroleum reservoirs, in addition to effects on saturated permeability, cataclasis in poorly lithified sediments will make these structures more likely to act as capillary barriers.

6. Conclusions

Based on microstructural observations, grain surface textures, and PSD measurements of undeformed and deformed sediments from the Sand Hill fault zone and small-displacement deformation band shear zones, we note that the mechanism of cataclasis in poorly lithified sediments is different from constrained comminution. The style of grain breakage is dependent on relative grain strength. From strongest to weakest:

1. Quartz deformation was accomplished by flaking or spalling of small chips from the perimeters of grains.
2. Feldspars deformed by transgranular fracturing, facilitated by their strong cleavage.
3. Volcanic lithic grains deformed primarily by distributed microcracking and to a lesser extent, transgranular fracturing.

Deformation preferentially removes intermediate sized particles, resulting in a progressive flattening of the original PSDs. The PSDs of all of the deformation band shear zone samples can be described by power law relations, with D values of 1.7–2.1. These values are lower than those predicted by the constrained comminution model, and indicate a preponderance of large particles. The shapes and D values of the PSDs are affected by the low confining pressures (20–30 MPa), the mineralogical dependence of grain breakage, and the compositionally immature nature of the sediments. We infer that deformation in these poorly lithified sediments occurred by controlled particulate flow. The cataclasis facilitated extensive grain boundary sliding, which accommodated the majority of the deformation. As the heavily faulted extensional basins of the western United States are filled with immature, poorly lithified sediments similar to the Santa Fe Group, we expect these conclusions to be generally applicable to many other fault zones. The implications of this mechanism of cataclasis for cross-fault fluid flow in these environments is profound, as the resulting structures have significantly reduced saturated permeability compared with their host sediments (Sigda et al., 1999; Rawling et al., 2001).

Acknowledgements

Support was provided by the National Science Foundation (grants EAR 9706482 and EAR 9526983) and the New Mexico Geological Society. Thorough reviews by Julia Morgan and Haakon Fossen, and comments from Editor Jim Evans, greatly improved the manuscript. We are grateful to William Stone for discussions on data analysis, Sean Connell for discussions on Santa Fe group stratigraphy, Nelia Dunbar and Lynn Heizler for assistance with the microprobe, Bruce Harrison for the use of his lab, and the U.S. Fish and Wildlife Service and Burlington Northern Santa Fe Railroad for granting access to the Bosque del Apache site. We thank Andy Dunn for the sieve analysis and Matt Herrin for providing sediment compositional data.

References

An, L.-j., Sammis, C., 1994. Particle size distribution of cataclastic fault materials from southern California: a 3-d study. Pure and Applied Geophysics 143, 203–227.

Antonellini, M., Aydin, A., 1995. Effect of faulting on fluid flow in porous sandstones: geometry and spatial distribution. American Association of Petroleum Geologists Bulletin 79, 642–671.

Antonellini, M.A., Aydin, A., Pollard, D.A., 1994. Microstrucuture of deformation bands in porous sandstones at Arches National Park, Utah. Journal of Structural Geology 16, 941–959.

Aydin, A., 1978. Small faults formed as deformation bands in sandstones. Pure and Applied Geophysics 116, 913–930.

Aydin, A., Johnson, A.M., 1978. Development of faults as zones of deformation bands and as slip surfaces in sandstone. Pure and Applied Geophysics 116, 931–942.

Beckner, J., 1996. Cementation processes and sand petrography of the Zia Formation, Albuquerque Basin, New Mexico. M.S. thesis, New Mexico Institute of Mining and Technology.

Beckner, J., Mozley, P.S., 1998. Origin and spatial distribution of early phreatic and vadose calcite cements in the Zia formation, Albuquerque Basin, New Mexico, USA. In: Morad, S. (Ed.), Carbonate Cements in Sandstones. International Association of Sedimentologists Special Publication 26, pp. 27–51.

Been, K., Jefferies, M.G., Hachey, J., 1991. The critical state of sands. Geotechnique 41, 365–381.

Biegel, R.L., Sammis, C.G., Dieterich, J.H., 1989. The frictional properties of simulated gouge having a fractal particle distribution. Journal of Structural Geology 11, 827–846.

Blenkinsop, T.G., 1991. Cataclasis and processes of particle size reduction. Pure and Applied Geophysics 136, 59–86.

Blenkinsop, T.G., Rutter, E.H., 1986. Cataclastic deformation of quartzite in the Moine Thrust Zone. Journal of Structural Geology 8, 669–682.

Borg, I., Friedman, M., Handin, J., Higgs, D.V., 1960. Experimental deformation of St. Peter sand: a study of cataclastic flow. In: Griggs, D., Handin, J. (Eds.), Rock Deformation. Geological Society of America Memoir 79, pp. 133–191.

Borradaile, G.J., 1981. Particulate flow of rock and the formation of cleavage. Tectonophysics 72, 305–321.

Byrne, T., 1994. Sediment deformation, dewatering and diagenesis: illustrations from selected melange zones. In: Maltman, A. (Ed.). The Geological Deformation of Sediments. Chapman & Hall, pp. 239–260.

Caine, J.S., Evans, J.P., Forster, C.B., 1996. Fault zone architecture and permeability structure. Geology 24, 1025–1028.

Cashman, S., Cashman, K., 2000. Cataclasis and deformation-band formation in unconsolidated marine-terrace sand, Humboldt County, California. Geology 28, 111–114.

Connell, S.D., Koning, D.J, Cather, S.M., 1999. Revisions to the stratigraphic nomenclature of the Santa Fe Group, northwestern Albuquerque Basin, New Mexico. In: Pazzaglia, F.J., Lucas, S.G. (Eds.), Albuquerque Geology. New Mexico Geological Society Guidebook 50, pp. 337–353.

Dunn, D.E., LaFountain, L.J., Jackson, R.E., 1973. Porosity dependence and mechanism of brittle fracture in sandstones. Journal of Geophysical Research 78, 2403–2417.

Ellen, S.D., Fleming, R.W., 1987. Mobilization of debris flows from soil slips, San Francisco Bay region, California. In: Costa, J.E., Wieczorek, G.F. (Eds.), Debris Flows/Avalanches: Process, Recognition, and Mitigation. Geological Society of America Reviews in Engineering Geology 7, pp. 31–40.

Engelder, J.T., 1974. Cataclasis and the generation of fault gouge. Geological Society of America Bulletin 85, 1515–1522.

Folk, R.L., 1974. Petrology of Sedimentary Rocks. Hemphill, Austin, TX.

Hawley, J.W., 1996. Hydrogeologic framework of potential recharge areas in the Albuquerque basin, central New Mexico. New Mexico Bureau of Mines and Mineral Resources Open-File Report 402 D, Chapter 1.

Hawley, J.W., Haase, C.S., Lozinsky, R.P., 1995. An underground view of the Albuquerque basin, In: Proceedings, 39th Annual Water Conference. New Mexico Water Resources Research Institute Report 290, pp. 37–55.

Herrin, M., 2001. Characteristics of deformation bands in poorly lithified sand, Rio Grande rift, New Mexico. M.S. Thesis, New Mexico Institute of Mining and Technology.

Heynekamp, M.R., Goodwin, L.B., Mozley, P.S., Haneberg, W.C., 1999. Controls on fault-zone architecture in poorly lithified sediments, Rio Grande Rift, New Mexico: implications for fault-zone permeability and fluid flow. In: Haneberg, W.C., Mozley, P.S., Moore, K.C., Goodwin, L.B. (Eds.), Faults and Subsurface Fluid Flow in the Shallow Crust. American Geophysical Union Geophysical Monograph 113, pp. 27–50.

Hooke, R.L., Iverson, N.R., 1995. Grain-size distribution in deforming subglacial tills: role of grain fracture. Geology 23, 57–60.

Kennedy, S.K., Mazzulo, J., 1991. Image analysis method of grain size measurement. In: Syvitski, J.P.M. (Ed.). Principles, Methods, and Application of Particle Size Analysis. Cambridge University Press, pp. 76–87.

Krinsley, D.H., Doornkamp, J.C., 1973. Atlas of Quartz Sand Surface Textures. Cambridge University Press, Cambridge.

Krinsley, D.H., Marshall, J.R., 1987. Sand grain textural analysis: an assessment. In: Marshall, J.R. (Ed.). Clastic Particles. Van Nostrand Reinhold Company, New York, pp. 2–15.

Lucas, S.E., Moore, J.C., 1986. Cataclastic deformation in accretionary wedges: Deep Sea Drilling Project Leg 166, southern Mexico, and on-land examples from Barbados and Kodiak Islands. In: Moore, J.C. (Ed.), Structural Fabrics in Deep Sea Drilling Project Cores from Forearcs. Geological Society of America Memoir 166, pp. 89–104.

Mandl, G., de Jong, L.N.J., Maltha, A., 1977. Shear zones in granular material: an experimental study of their structure and genesis. Rock Mechanics 9, 95–144.

Marone, C., Scholz, C.H., 1989. Particle-size distribution and microstructures within simulated fault gouge. Journal of Structural Geology 11, 799–814.

Mazzulo, J., Kennedy, S.K., 1985. Automated measurement of the nominal sectional diameters of individual sedimentary particles. Journal of Sedimentary Petrology 55, 593–595.

McCave, I.N., Syvitski, J.P.M., 1991. Principles and methods of geological particle size analysis. In: Syvitski, J.P.M. (Ed.). Principles, Methods, and Application of Particle Size Analysis. Cambridge University Press, pp. 3–22.

Menéndez, B., Zhu, W., Wong, T.-f., 1996. Micromechanics of brittle faulting and cataclastic flow in Berea sandstone. Journal of Structural Geology 18, 1–16.

Mozley, P.S., Goodwin, L.B., 1995. Patterns of cementation along a Cenozoic normal fault: a record of paleoflow orientations. Geology 23, 539–542.

Porter, J.R., Knipe, R.J., Fisher, Q.J., Farmer, A.B., Allin, N.S., Jones, L.S., Palfrey, A.J., Garrett, S.W., Lewis, G., 2000. Deformation processes in the Britannia Field, UKCS. Petroleum Geoscience 6, 241–254.

Rawling, G.C., Goodwin, L.B., Wilson, J.L., 2001. Internal architecture, permeability structure, and hydrologic significance of contrasting fault-zone types. Geology 29, 43–46.

Russ, J.C., 1991. Practical Stereology. Plenum Press, New York.

Russ, J.C., 1999. The Image Processing Handbook. CRC Press, Boca Raton, FL.

Sammis, C., King, G., Biegel, R., 1987. The kinematics of gouge deformation. Pure and Applied Geophysics 125, 777–812.

Sibson, R.H., 1977. Fault rocks and fault mechanisms. Journal of the Geological Society of London 133, 191–213.

Sigda, J.M., Goodwin, L.B., Mozley, P.S., Wilson, J.L., 1999. Permeability alteration in small-displacement faults in poorly lithified sediments: Rio Grande Rift, Central New Mexico. In: Haneberg, W.C., Mozley, P.S., Moore, K.C., Goodwin, L.B. (Eds.), Faults and Subsurface Fluid Flow in the Shallow Crust. American Geophysical Union Geophysical Monograph 113, pp. 51–68.

Tedford, R.H., Barghoorn, S., 1999. Santa Fe Group (Neogene), Ceja del Rio Puerco, Northwestern Albuquerque Basin, Sandoval County, New Mexico. In: Pazzaglia, F.J., Lucas, S.G. (Eds.), Albuquerque Geology. New Mexico Geological Society Guidebook 50, pp. 327–335.

Turcotte, D.L., Huang, J., 1995. Fractal distributions in geology, scale invariance, and deterministic chaos. In: Barton, C.C., La Pointe, P.R. (Eds.). Fractals in the Earth Sciences. Plenum Press, New York, pp. 1–40.

Underhill, J.R., Woodcock, N.H., 1987. Faulting mechanisms in high-porosity sandstones; New Red Sandstone, Arran, Scotland. In: Jones, M.E., Preston, R.M.F. (Eds.), Deformation of Sediments and Sedimentary Rocks. Geological Society of London Special Publication 29, pp. 91–105.

Whitworth, T.M., Haneberg, W.C., Mozley, P.S., Goodwin, L.B., 1999. Solute-sieving induced calcite precipitation on pulverized quartz sand: experimental results and implications for membrane behavior of fault gouge. In: Haneberg, W.C., Mozley, P.S., Moore, K.C., Goodwin, L.B. (Eds.), Faults and Subsurface Fluid Flow in the Shallow Crust. American Geophysical Union Geophysical Monograph 113, pp. 149–158.

Wilson, E.B., 1952. An Introduction to Scientific Research. McGraw-Hill, New York.

Wong, T.-f., David, C., Zhu, W., 1997. The transition from brittle faulting to cataclastic flow in porous sandstones: mechanical deformation. Journal of Geophysical Research 102, 3009–3025.

Zhang, J., Wong, T.-f., Davis, D.M., 1990. Micromechanics of pressure-induced grain crushing in porous rocks. Journal of Geophysical Research 95, 341–352.